White Hole Analogs in
Circular Hydraulic Jumps:
An Experimental Study

Kartik Tiwari
Submitted in fulfillment of an Independent Study Module
7 November 2022

Contents

Acknowledgements

Figure 1: Image of a circular hydraulic jump captured while conducting the experiment

1. **Introduction**

In this project, I explore elements of fluid mechanics and general relativity to develop my understanding of analog gravity. In particular, I explore the theoretical framework underlying processes that enable us to map certain properties of time-reversed blackholes (i.e. white-holes) onto the circular hydraulic jump. Following this, I discuss the experiment that I performed to verify some of the theoretical predictions.

1.1 *Analog Gravity*

Experiments to test features of general relativity are notoriously hard to perform - especially at an undergraduate level. Often, we only hear about large-scale big budget experiments to probe GR like the Event Horizon Telescope, Gravitational Waves Interferometry, etc. Manipulating spacetime curvature in any observationally significant sense requires at least planetary mass-scales. However, advancements in analog models of general relativity in the recent past have provided hopes of studying important GR features in a laboratory setting. Several analog models have been developed under different physical frameworks (such as laser pulse analogs, Bose-Einstein condensate analogs, etc.). Within each framework, there are further several models with varying interesting features. What I will be concerning myself with is to study the circular hydraulic jump in fluid mechanics

that, as I would demonstrate, is an analog model for time reversed Schwarzschild geometry.

1.2   *Circular Hydraulic Jump*

When a jet of liquid impacts a surface, under suitable conditions there is an abrupt increase in the height of the fluid (see Fig. 1). This phenomena is known as the circular hydraulic jump. For over a century, it was believed that all kinds of circular hydraulic jump were caused due to gravity. However, recent experimental demonstration and analytic treatment by Bhagat et al. demonstrated that thin film hydraulic jumps result when surface tension and viscous forces balance the fluid momentum (without gravity playing a significant role). From their fairly subtle analytic treatment, one deduces that the circular jump occurs when there is a singularity which satisfies the following expression.

$$\frac{1}{We} + \frac{1}{Fr^2} = 1 \tag{1}$$

where We stands for Webber number and Fr stands for Froude number.

2.   **Uncovering the Analogy**

Informally, it is easy to have a superficial intuition of how the circular hydraulic jump maps onto 2+1 white hole geometries. However, to arrive at a rigorous and conceptually sound understanding of the system, we need to assemble various different pieces. In this section, I will derive various results - some quite well known and some not as famous - and use them to demonstrate the usefulness of the acoustic analog in understanding GR.

2.1   *Pieces from Fluid Mechanics*

2.1.1   Dispersion Relation of Gravity Waves

The broad outline of the project in this section is the following. We would first make certain assumptions in order to arrive at the equation of motion for the surface gravity waves. Then, we would argue on physical grounds to get three boundary conditions. Following this, we would linearize the problem and finally extract the dispersion relation.

In fluid mechanics, the Convective Time Derivative (i.e. the time derivative in the local rest frame of the fluid) is defined as

$$\frac{D}{Dt} = \frac{\partial}{\partial t} + (\vec{v}.\nabla) \tag{2}$$

In fluid mechanics, the continuity equation is written as

$$\frac{\partial \rho}{\partial t} + \nabla.(\rho \vec{v}) = 0 \tag{3}$$

$$\implies \frac{\partial \rho}{\partial t} + (\vec{v}.\nabla)\rho = -(\rho\nabla).\vec{v} \tag{4}$$

In terms of convective time derivative, then, we can write -

$$\frac{D\rho}{Dt} = \left(\frac{\partial}{\partial t} + (\vec{v}.\nabla)\right)\rho = -(\nabla\vec{v})\rho \tag{5}$$

So we re-write the continuity equation as

$$\frac{1}{\rho}\frac{D\rho}{Dt} = -\nabla\vec{v} \tag{6}$$

If the fluid is incompressible, this must mean that the mass density of a co-moving volume element does not change with time. So we get a divergence free velocity field for the liquid

$$\frac{D\rho}{Dt} = 0 \implies \nabla\vec{v} = 0 \tag{7}$$

Suppose the force acting on the liquid is conservative (like gravity). Then we can write the force as as the gradient of potential energy Φ

$$\vec{F} = -\nabla\Phi \tag{8}$$

If we define potential energy per unit mass as $\Psi = \Phi/m \implies \Phi = m\Psi$ then we can write potential energy per unit volume as $\Phi/V = (m/V)\Psi = \rho\Psi$. So, we can write the force per unit volume as

$$\vec{F_V} = \vec{F}/V = -\rho\nabla\Psi \tag{9}$$

Further, assuming constant viscosity, we have the Navier Stokes equation (Derive this in an appendix section) -

$$\frac{D\vec{v}}{Dt} = -\frac{\nabla p}{\rho} - \nabla\psi + \nu\nabla^2\vec{v} \tag{10}$$

where the ratio of viscosity[1] to density $\nu = \mu/\rho$ is the kinematic viscosity (with units of m^2/s) and gives a rough measure of momentum diffusion. Also, $p = p(\vec{r}, t)$ is the total pressure. This is also known as the non-linear Euler equation.

Now we have two equations that govern the flow of incompressible fluids in presence of conservative volume forces.

$$\boxed{\nabla.\vec{v} = 0 \text{ and } \frac{D\vec{v}}{Dt} = -\frac{\nabla p}{\rho} - \nabla\psi + \nu\nabla^2\vec{v}}$$

---

[1]Viscosity is the constant of proportionality between the shear rate and the tangential force per unit area when parallel planes are sliding over each other.

We can plug in the the potential energy per unit mass due to gravity ($\Psi = gz$) and expand the convective time derivative of the second equation to get

$$\frac{\partial \vec{v}}{\partial t} + (\vec{v}.\nabla)\vec{v} = -\frac{\nabla p}{\rho} - g\hat{z} + \frac{\mu}{\rho}\nabla^2\vec{v} \tag{11}$$

or, on rearranging

$$\rho\frac{\partial \vec{v}}{\partial t} + \rho(\vec{v}.\nabla)\vec{v} = -\nabla p - \rho g\hat{z} + \mu\nabla^2\vec{v} \tag{12}$$

In general, the total pressure can have three components

$$p = p_0 - \rho gz + p_1(\vec{r}, t) \tag{13}$$

where p_0 is the atmospheric pressure and p_1 is the pressure perturbation due to the wave. Substituting this p back into Eq. 12

$$\rho\frac{\partial \vec{v}}{\partial t} + \rho(\vec{v}.\nabla)\vec{v} = -\nabla(p_0 - \rho gz + p_1) - \rho g\hat{z} + \mu\nabla^2\vec{v} \tag{14}$$

$$\rho\frac{\partial \vec{v}}{\partial t} + \rho(\vec{v}.\nabla)\vec{v} = \rho g\hat{z} - \nabla p_1 - \rho g\hat{z} + \mu\nabla^2\vec{v} \tag{15}$$

$$\rho\frac{\partial \vec{v}}{\partial t} + \rho(\vec{v}.\nabla)\vec{v} = -\nabla p_1 + \mu\nabla^2\vec{v} \tag{16}$$

If we neglect the small terms (in v^2), then we can approximate

$$\rho\frac{\partial \vec{v}}{\partial t} \approx -\nabla p_1 + \mu\nabla^2\vec{v} \tag{17}$$

Further, if the wavelength is not very small, then we can also neglect the viscosity term

$$\rho\frac{\partial \vec{v}}{\partial t} \approx -\nabla p_1 \tag{18}$$

Taking the curl of this equation

$$\nabla \times \left(\rho\frac{\partial \vec{v}}{\partial t}\right) = \nabla \times (-\nabla p_1) \tag{19}$$

From vector calculus, we know curl of a gradient is zero. We take density of the fluid to be non-zero. So it follows,

$$\frac{\partial}{\partial t}(\nabla \times \vec{v}) = \frac{\partial w}{\partial t} = 0 \tag{20}$$

where curl of the velocity flow defines the vorticity ($\vec{w} = \nabla \times \vec{v}$). This establishes that the flow is irrotational. Irrotational flow implies that we can write the velocity as the gradient of a velocity potential.

$$\vec{v} = -\nabla\phi(\vec{r}, t) \tag{21}$$

From Eq. 7, we also know the velocity field is divergence free. So, taking the divergence of the previous expression, we arrive at

$$\nabla . \vec{v} = \nabla . (-\nabla \phi) = 0 \tag{22}$$

This means that the velocity potential satisfies Laplace equation.

$$\nabla^2 \phi = 0 \tag{23}$$

Also, rewriting Eq. 18 to relate velocity potential with dynamic pressure

$$\rho \frac{\partial (-\nabla \phi)}{\partial t} = -\nabla p_1 \tag{24}$$

$$\nabla \left(\rho \frac{\partial \phi}{\partial t} \right) = \nabla p_1 \implies \rho \frac{\partial \phi}{\partial t} = p_1 \tag{25}$$

Now we must look at the physics of the system to infer appropriate boundary conditions. In doing so, a schematic diagram might be of help. Assuming the rigid surface at the bottom is located at $z = -h$ (assuming constant depth), then the projection of the velocity on the normal direction at the bottom must vanish.

$$v_z \hat{z} = 0 \text{ at } z = -h \tag{26}$$

which implies

$$\frac{\partial \phi}{\partial z} = 0 \text{ at } z = -h \tag{27}$$

This is our first boundary condition. It is known as the kinematic bottom boundary condition.

We will try to get two boundary conditions from it - one kinematic (related to velocity) and one dynamic (related to forces). First, let ξ represent the vertical displacement of the free surface from $z = 0$ level due to the wave. Then, for a gently sloping free surface, it follows that the vertical velocity of the fluid on the surface would be equal to the vertical velocity of the surface itself. We can express this mathematically as

$$\frac{\partial \xi}{\partial t} = \frac{\partial \phi}{\partial z} \text{ at z = 0} \tag{28}$$

This is our second boundary condition, which we shall call the kinematic surface boundary condition.

Finally, we get to the most subtle boundary condition - the dynamic surface boundary condition. Most standard treatments of this aspect ignore the role of surface tension. For our purposes, however, the term that we get from surface tension plays an important role while mapping the dispersion relation to Schwarzschild metric.

To include surface tension, we create a model with a thin film covering the surface of the fluid

with surface tension T. If we consider a horizontal rectangle $dxdy$ on the free surface, then the net vertical force from four sides is

$$T\left(\frac{\partial\xi}{\partial x}\bigg|_{x+dx} - \frac{\partial\xi}{\partial x}\bigg|_{x}\right)dy + T\left(\frac{\partial\xi}{\partial y}\bigg|_{y+dy} - \frac{\partial\xi}{\partial y}\bigg|_{y}\right)dx = T\left(\frac{\partial^2\xi}{\partial x^2} + \frac{\partial^2\xi}{\partial y^2}\right)dxdy \tag{29}$$

There must be continuity of vertical force at the surface. Equating the pressure at $\xi + dz$ with pressure at $\xi - dz$ gives us

$$p_0 - \rho g z - p_1 + T\left(\frac{\partial^2\xi}{\partial x^2} + \frac{\partial^2\xi}{\partial y^2}\right) = p_0 \tag{30}$$

But at the surface $z = \xi$ and p_1 was solved for in Eq. 25. We can, therefore, write

$$-\rho g\xi - \rho\frac{\partial\phi}{\partial t} + T\left(\frac{\partial^2\xi}{\partial x^2} + \frac{\partial^2\xi}{\partial y^2}\right) = 0 \text{ at } z = 0 \tag{31}$$

We can further utilize the result of Eq. 28 from kinematic surface boundary condition. On differentiating the previous equation with time

$$g\frac{d\xi}{dt} + \frac{\partial^2\phi}{\partial t^2} - \frac{T}{\rho}\frac{d}{dt}\left(\frac{\partial^2\xi}{\partial x^2} + \frac{\partial^2\xi}{\partial y^2}\right) = 0 \text{ at } z = 0 \tag{32}$$

$$\implies g\frac{\partial\phi}{\partial z} + \frac{\partial^2\phi}{\partial t^2} - \frac{T}{\rho}\nabla^2.\left(\frac{\partial\phi}{\partial z}\right) = 0 \text{ at } z = 0 \tag{33}$$

This is the dynamic surface boundary condition.

Now, we plug in the ansatz for a wave like solution of the Laplace equation Eq. 23. Assuming the motion is in (x, z) plane, we can write the equation for wavetrain advancing along x direction with frequency ω, wave number k and an amplitude governed by the function $F(z)$.

$$\phi = F(z)e^{i(kx-\omega t)} \tag{34}$$

Our main task now is to fix the function $F(z)$.

First let us plug our ansatz in the Laplace equation to get the arrive at the general form of $F(z)$.

$$\nabla^2(\phi) = \left(\frac{\partial^2}{\partial x^2} + \frac{\partial^2}{\partial y^2} + \frac{\partial^2}{\partial z^2}\right)\phi = 0 \tag{35}$$

$$\left(\frac{\partial^2}{\partial x^2} + \frac{\partial^2}{\partial y^2} + \frac{\partial^2}{\partial z^2}\right)F(z)e^{i(kx-\omega t)} = 0 \tag{36}$$

$$F(z)\frac{\partial^2}{\partial x^2}e^{i(kx-\omega t)} + e^{i(kx-\omega t)}\frac{\partial^2}{\partial z^2}F(z) = 0 \tag{37}$$

$$F(z)(ik)^2 e^{i(kx-\omega t)} + e^{i(kx-\omega t)} F''(z) = 0 \tag{38}$$

Which gives us a second order ODE for $F(z)$

$$F'' - k^2 F = 0 \tag{39}$$

Clearly, the general solution to this ODE is of the following form [2]

$$F(z) = Ae^{kz} + Be^{-kz} \tag{40}$$

We can easily verify this ansatz.

$$F''(z) = A(k^2)e^{kz} + B(-k^2)e^{-kz} = k^2 F(z) \tag{41}$$

Currently, we have two unknown constants. To fix one, we can plug Eq. 40 back into the kinematic bottom boundary condition (i.e. Eq. 27).

$$\frac{\partial \phi}{\partial z} = e^{i(kx-\omega t)} \frac{d}{dz} F(z) \bigg|_{(z=-h)} = 0 \tag{42}$$

$$Ake^{kh} - Bke^{-kh} = 0 \tag{43}$$

$$A = Be^{-2kh} \tag{44}$$

Now, the form of our velocity potential is

$$\phi(x, z, t) = Ae^{kz} e^{i(kx-\omega t)} + Be^{-kz} e^{i(kx-\omega t)} \tag{45}$$

$$\phi(x, z, t) = A(e^{kz} + e^{-k(z+2h)}) e^{i(kx-\omega t)} \tag{46}$$

Now, to arrive at the dispersion relation, we simply have to plug this velocity potential in our dynamic surface boundary condition Eq. 33. So, at $z = 0$

$$gAe^{i(kx-\omega t)} \frac{\partial}{\partial z}(e^{kz} + e^{-k(z+2h)}) + A(e^{kz} + e^{-k(z+2h)}) \frac{\partial^2}{\partial t^2} e^{i(kx-\omega t)} - \\ \frac{T}{\rho} \nabla^2 \left(Ae^{i(kx-\omega t)} \frac{\partial}{\partial z}(e^{kz} + e^{-k(z+2h)}) \right) = 0 \tag{47}$$

Here one is confronted with some messy algebra but if we go through the steps carefully we should arrive at the required expression.

$$gke^{i(kx-\omega t)}(1 - e^{-2kh}) + (1 + e^{-2kh})(-i\omega)^2 e^{i(kx-\omega t)} - \frac{Tk}{\rho}(1 - e^{-2kh}) \nabla^2 \left(e^{i(kx-\omega t)} \right) = 0 \tag{48}$$

---

[2]Equivalently, we could also work with hyperbolic trigonometric functions as the ansatz of the ODE

$$gke^{i(kx-\omega t)}(1-e^{-2kh}) - \frac{Tk}{\rho}(1-e^{-2kh})\frac{\partial^2}{\partial x^2}\left(e^{i(kx-\omega t)}\right) = \omega^2(1+e^{-2kh})e^{i(kx-\omega t)} \qquad (49)$$

$$gke^{i(kx-\omega t)}(1-e^{-2kh}) - \frac{Tk}{\rho}(1-e^{-2kh})(ik)^2\left(e^{i(kx-\omega t)}\right) = \omega^2(1+e^{-2kh})e^{i(kx-\omega t)} \qquad (50)$$

$$gk(1-e^{-2kh}) + \frac{Tk^3}{\rho}(1-e^{-2kh}) = \omega^2(1+e^{-2kh}) \qquad (51)$$

This finally gives our dispersion relation

$$\omega^2 = \frac{(1-e^{-2kh})}{(1+e^{-2kh})}\left(gk + \frac{Tk^3}{\rho}\right) \qquad (52)$$

Recall the definitions of hyperbolic trigonometric functions

$$\cosh x = \frac{1}{2}(e^x + e^{-x}) \text{ and } \sinh x = \frac{1}{2}(e^x - e^{-x}) \qquad (53)$$

This gives us the definition of hyperbolic tangent function

$$\tanh x = \frac{e^x - e^{-x}}{e^x + e^{-x}} \qquad (54)$$

If we divide the numerator and denominator of the RHS by e^x, we will get the following form

$$\tanh x = \frac{e^x - e^{-x}}{e^x + e^{-x}} \times \frac{(1/e^x)}{(1/e^x)} = \frac{1 - e^{-2x}}{1 + e^{-2x}} \qquad (55)$$

Comparing this form of the hyperbolic tan function with the dispersion relation expression, we can write

$$\boxed{\omega^2 = \left(gk + \frac{Tk^3}{\rho}\right)\tanh(kh)}$$

2.1.2 Shallow Depth - Long Wavelength Limit

In the case of shallow water where the depth of water is much less than the relevant wavelength ($h << \lambda = 2\pi/k$), we can use the taylor expansion of $\tanh x$ to simplify the dispersion relation.

$$\tanh x \approx x - \frac{1}{3}x^3 + \mathcal{O}(x^5)... \qquad (56)$$

Truncating at the cubic power and plugging the expansion into the dispersion relation gives

$$\omega^2 = \left(gk + \frac{Tk^3}{\rho}\right)\left(kh - \frac{1}{3}(kh)^3...\right) \qquad (57)$$

$$\omega^2 \approx ghk^2 - \frac{1}{3}gh^3k^4 + \frac{Tk^4h}{\rho} + \frac{Th^3k^6}{3\rho} \tag{58}$$

Truncating at the k^4 power will give us

$$\omega^2 = (gh)k^2 + (gh)k^4\left(\frac{T}{g\rho} - \frac{1}{3}h^2\right) \tag{59}$$

The quantity $\sqrt{T/g\rho}$ is known as the capillary length l_c of the fluid. So, in terms of capillary length, we can write the shallow depth long wavelength approximation of dispersion relation as

$$\omega^2 = (gh)k^2 + (gh)k^4\left(l_c^2 - \frac{1}{3}h^2\right) \tag{60}$$

If we calculate the phase velocity $v_p = \omega/k$ we find

$$v_p^2 = \frac{\omega^2}{k^2} = (gh) + (gh)k^2\left(l_c^2 - \frac{1}{3}h^2\right) \tag{61}$$

For long wavelength, shallow depth and small capillary lengths, we can approximate the phase velocity to the first order as a constant

$$v_p = \sqrt{gh} \tag{62}$$

Therefore, the dispersion relation can be written as

$$\omega^2 = v_p^2 k^2 + v_p^2 k^4\left(l_c^2 - \frac{1}{3}h^2\right) \tag{63}$$

2.1.3 Ripplon Metric (Geometric Argument)

Now, consider a point source emitting surface waves [3] radially outwards while floating along a moving fluid medium (as depicted in Fig. 2). After sometime dt the pulse emitted would form a spherical shell of radius $\vec{v_p}dt$ surrounding the point source (which would have been dragged by the moving fluid). The point source would have moved from its original position (which we take to be the origin) by some distance $\vec{v_s}dt$ (where $\vec{v_s}$ is the surface velocity of the fluid).

Now, the location of the shell measured in the direction of fluid flow with respect to the original position of the point source (denoted by $\vec{dx}$) can be found by solving the following equation

$$|\vec{dx} - \vec{v_s}dt| = \vec{v_p}dt \tag{64}$$

---

[3]Note that one can trace a similar argument using sound waves instead of surface gravity waves
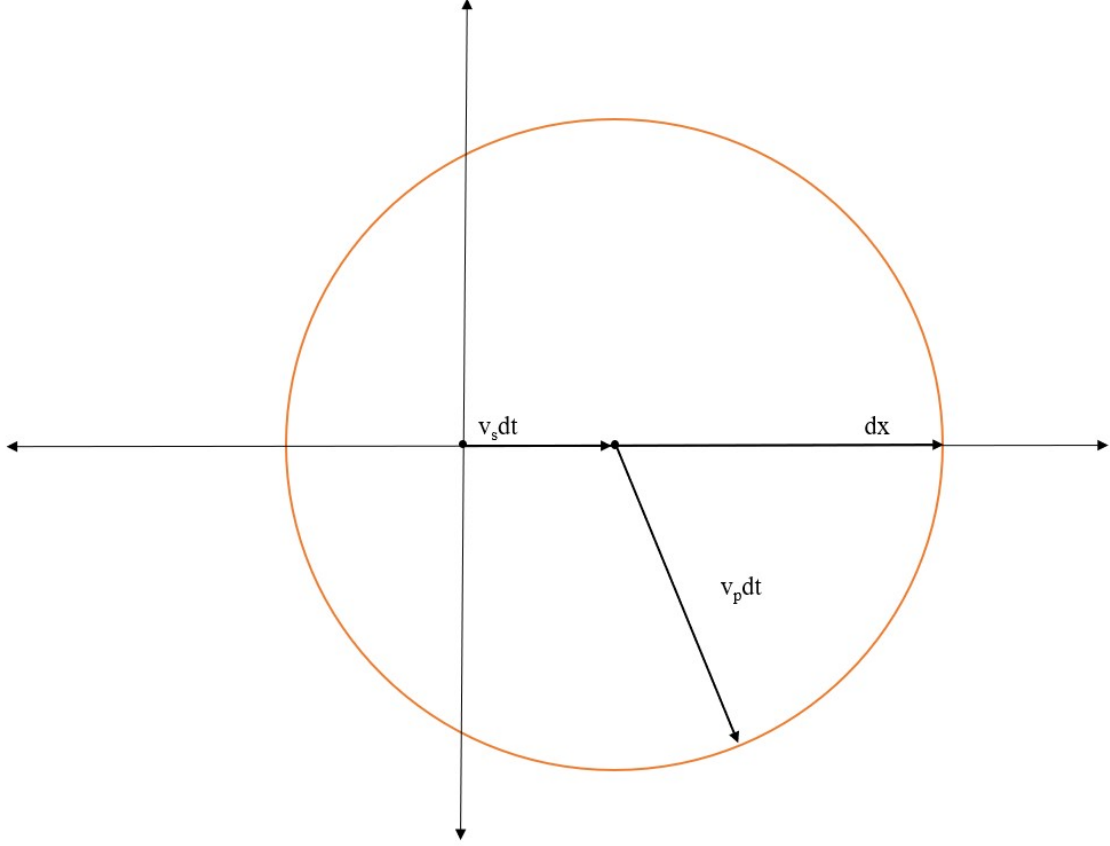
Figure 2: Orange circle represents the spherical shell at some time $t_0 + dt$ formed by the wave pulse emitted at some time t_0. The point source at t_0 was located at the origin but is now at some position $\vec{v_s}dt$ because it was dragged by the surface flow of the fluid medium. Wave pulse would have travelled some distance $\vec{v_p}dt$ radially outwards (where v_p is the phase velocity).

On squaring the equation and expanding

$$d\vec{x}^2 + (\vec{v_s}dt)^2 - 2\vec{v_s}d\vec{x}dt = (\vec{v_p}dt)^2 \tag{65}$$

On collecting terms,

$$-(\vec{v_p}^2 - \vec{v_s}^2)dt^2 - 2\vec{v_s}d\vec{x}dt + d\vec{x}^2 = 0 \tag{66}$$

Notice how we can infer a spacetime rippplon metric from the previous expression.

$$g_{\mu\nu} \propto \begin{pmatrix} -(v_p^2 - v_s^2) & -(v_s)_i \\ -(v_s)_i & \delta_{ij} \end{pmatrix} \tag{67}$$

Where δ_{ij} is the kronecker delta function[4], $(v_s)_i$ represents the surface velocity component in the

---

[4]Note that the submatrix is only an identity matrix in cartesian coordinates. In other radial coordinate systems,

i^{th} direction and v_p is the phase velocity of ripplons (that remains constant).

In terms of this ripplon metric, Eq. 66 clearly shows that ripplons travel along null geodesics.

$$ds^2 = 0 \implies g_{\mu\nu}dX^\mu dX^\nu = 0 \tag{68}$$

Because the metric is static, we can also say

$$g_{\mu\nu}\frac{dX^\mu}{dt}\frac{dX^\nu}{dt} = 0 \tag{69}$$

which is just the statement that ripplons travel with phase velocity with respect to the co-moving reference frame.

Even though the underlying framework governing the system (i.e. machinery of fluid mechanics like continuity equation, Euler's equation etc.) is completely non-relativistic, we can get space and time on the same footing because the ripplons nevertheless couple to a spacetime metric that places space and time in a unified framework.

> Notice that in Eq. 67 we only arrived at a proportionality for the metric and not its exact form. This is a subtle point. Though the geometric argument is quite easy to follow (almost trivial), it has the disadvantage of not being sufficient to determine an overall position dependant conformal factor. In order to fix the conformal factor, we will need to use the **Physical Argument** (instead of the geometrical one) and treat the waves (either sound or ripples) as perturbations on a fixed scalar field and then assembles two first order differential equations and one equation of state into one second order equation (i.e. the *Klein-Fock-Gordon Equation*) that represents general wave motion using a spacetime metric.

2.2 *Pieces from General Relativity*

2.2.1 Role of Coordinate Choices in Schwarzschild Metric

It is well known that the Schwarzschild metric Eq. 70 is a vacuum solution for Einstein's field equation in the presence of an uncharged spherically symmetric mass distribution. Though the derivation is quite subtle and involved, considering it is a standard result, it can be found in any textbook on general relativity.

$$ds^2 = -\left(1 - \frac{2GM}{c^2 r}\right)c^2 dt^2 + \left(1 - \frac{2GM}{c^2 r}\right)^{-1} dr^2 + r^2 d\theta^2 + r^2 \sin^2\theta d\phi^2 \tag{70}$$

---

the matrix would have the corresponding Jacobian elements. However, regardless of the coordinate choice, the submatrix would always have a diagonal form.

Note how the values $r = 0$ and $r = 2GM/c^2$ lead to a blow up of metric coefficients. It is possible, however, that these singularities could be artifacts of our coordinate choices. For example, in a simple plane expressed in spherical coordinates $ds^2 = dr^2 + r^2 d\theta^2$ the origin $r = 0$ is degenerate which means the $g^{\theta\theta} = r^{-2}$ component of the inverse metric blows up - even though the origin has no special physical features.

What physical signature can be used to determine whether or not a singularity in metric components corresponds to a physical feature is a nuanced issue but one first guess would be to check for the curvature. Riemann curvature tensor does provide an account of curvature but its components are again coordinate dependant. However, we can construct the Ricci scalar by contracting the Ricci tensor (which we get using symmetry properties of Riemann tensor). On performing the scalar quantity check for infinite curvature, we see $r = 0$ is a true singularity and $r = 2GM/c^2$ is merely a coordinate singularity.

It is common practice in GR to perform appropriate coordinate transformations to rid ourselves of coordinate singularities. This brings us to a salient feature of discussing geometries of spacetime in general relativity- working under different coordinate systems can help in investigating different features of the physical system. For example, in-going and out-going Eddington-Finkelstein coordinates regularize future and past horizons (i.e. the shell at $r = 2GM/c^2$) by pushing them to $\pm\infty$ in Schwarzschild geometries respectively. One such coordinate choice which is extensively used in analog gravity is called *Painleve-Gullstrand* coordinates. In the following section, I would motivate and derive PG coordinates explicitly derive in their appropriate form

2.2.2 Transforming to Painleve-Gullstrand Coordinate

An in-falling observer would have no problem (conceptually speaking) in crossing the horizon $(r = 2GM/c^2)$ in some finite time interval. However, a distant observer who is keeping track of the position of in-falling observer would notice that it takes an infinite amount of time for the in-falling observer to actually cross the horizon. In other words, for a distant observer an object plunging into a black hole seems frozen at the horizon. We can prove this by considering radial (i.e. constant θ and ϕ) null geodesics in Schwarzschild spacetime $ds^2 = 0$.

$$0 = -\left(1 - \frac{r_s}{r}\right) c^2 dt^2 + \left(1 - \frac{r_s}{r}\right)^{-1} dr^2 \tag{71}$$

where I denote $r_s = 2GM/c^2$ as Schwarzschild radius. On rearranging the previous equation to get the slope of a light cone in a spacetime $(t - r)$ diagram.

$$\frac{cdt}{dr} = \left(1 - \frac{r_s}{r}\right)^{-1} \tag{72}$$

Clearly, as a light-cone approaches the horizon it starts to close up until it becomes a perpendicular line (i.e infinite slope) at r_s. We can try to fix this by adopting a time-coordinate that moves more slowly as we along null geodesics. So, let's define a new time coordinate in terms of our familiar older one

$$dt = dT - h(r)dr \tag{73}$$

and plug it back in the metric.

$$ds^2 = -\left(1 - \frac{r_s}{r}\right)c^2(dT^2 - 2h(r)drdt + h(r)^2dr^2) + \left(1 - \frac{r_s}{r}\right)^{-1}dr^2 + r^2d\Omega^2 \tag{74}$$

where $d\Omega^2 = d\theta^2 + \sin^2\theta d\phi^2$ is a 2-sphere. Now, we define $v^2 = r_s/r$ and expand the previous expression.

$$ds^2 = -(1 - v^2)c^2dT^2 + 2h(r)(1 - v^2)c^2drdT - (1 - v^2)c^2h(r)^2dr^2 + (1 - v^2)^{-1}dr^2 + r^2d\Omega^2 \tag{75}$$

On collecting the terms and rewriting

$$ds^2 = -(1 - v^2)c^2dT^2 + 2h(r)(1 - v^2)c^2drdT + \left(\frac{1}{(1 - v^2)} - (1 - v^2)c^2h(r)^2\right)dr^2 + r^2d\Omega^2 \tag{76}$$

Now, we wish to solve for the function $h(r)$. We do so by setting the coefficient of dr^2 term as 1. Therefore, we get

$$1 = \frac{1}{(1 - v^2)} - (1 - v^2)c^2h(r)^2 \tag{77}$$

$$1 - v^2 = 1 - (1 - v^2)^2c^2h(r)^2 \tag{78}$$

$$c^2h(r)^2 = \frac{v^2}{(1 - v^2)^2} \tag{79}$$

Therefore, we get

$$h(r) = \pm\frac{v(r)}{c(1 - v(r)^2)} \tag{80}$$

If we plug the form of $h(r)$ back into the metric in Eq. 76, we get the following simplified form

$$ds^2 = -(1 - v(r)^2)c^2dT^2 \pm 2cv(r)drdT + dr^2 + r^2d\Omega^2 \tag{81}$$

Suppose we are restricting ourselves to a 2+1 dimensional spacetime. Then we can write

$$ds^2 = -\left(1 - \frac{1}{c^2}\left(\frac{2GM}{r}\right)\right)c^2dT^2 \pm 2c\sqrt{\frac{2GM}{c^2r}}drdT + dr^2 + r^2d\theta^2 \tag{82}$$

$$ds^2 = -\left(c^2 - \left(\frac{2GM}{r}\right)\right)dT^2 \pm 2\sqrt{\frac{2GM}{r}}drdT + dr^2 + r^2d\theta^2 \tag{83}$$

Redefining $v(r)^2 = 2GM/r$ will give us

$$ds^2 = -(c^2 - v^2)dT^2 \pm 2vdrdT + dr^2 + r^2 d\theta^2$$

Notice, for this line element in Schwarzschild geometry, we can write the metric tensor as

$$g_{\mu\nu} = \begin{pmatrix} -(c^2 - v(r)^2) & \pm v(r) & 0 \\ \pm v(r) & 1 & 0 \\ 0 & 0 & r^2 \end{pmatrix} \tag{84}$$

Equivalently, in rectangular coordinates and generalizing to non-radial geodesics, we can say

$$g_{\mu\nu} = \begin{pmatrix} -(c^2 - v(x,y)^2) & \pm v_i(x,y) \\ \pm v_i(x,y) & \delta_{ij} \end{pmatrix} \tag{85}$$

The choice of $(+)$ sign corresponds to outgoing PG coordinates and $(-)$ sign corresponds to ingoing PG coordinates. Eq. 85 is written in such a way that *space* appears flat even though *spacetime* is curved.

2.3   Reflecting on the Results

Let's recall the three most important results that we have arrived at till now. First, we got the dispersion relation for surface gravity waves (ripplons) which - under suitable assumptions - provided us with a expression for phase velocity.

$$v_p = \sqrt{gh} \tag{86}$$

Then, we established the metric tensor associated with ripplon propagation (albeit as a proportionality and not an equality yet).

$$g_{\mu\nu}^{ripplon} \propto \begin{pmatrix} -(v_p^2 - v_s^2) & -(v_s)_i \\ -(v_s)_i & \delta_{ij} \end{pmatrix} \tag{87}$$

Finally, we transformed the metric tensor associated with Schwarzschild spacetime to ingoing Painleve Gullstrand coordinates and got

$$g_{\mu\nu}^{PG} = \begin{pmatrix} -(c^2 - v(x,y)^2) & -v_i(x,y) \\ -v_i(x,y) & \delta_{ij} \end{pmatrix} \tag{88}$$

Now, in order to mimic the schwarzschild metric, we need to find a form of fluid flow that meets the following requirements -

1. Phase velocity of the waves is position independent because locally measured speed of light is a position independent constant

2. The flow must be spherically symmetric [5]

Finally, for a complete identity between $g_{\mu\nu}^{PG}$ and $g_{\mu\nu}^{ripplon}$ we are required to fix the conformal factor. To do so, we must move to physical arguments for the ripplon metric and actually derive the wave-equation in the Klein-Gordon-Fock form. Due to some challenges posed by the conformal factor, we cannot have a complete identity between the two metrics. The closest we can arrive at is to find a fluid flow such that

$$g_{\mu\nu}^{ripplon} \propto g_{\mu\nu}^{PG} \tag{89}$$

In such an analog case, we can study all kinds of conformal invariants.

Now, notice Eq. 86 satisfies condition (1) for all ripplons. For a circular hydraulic jump, there is spherical symmetry of flow profile on a 2-D plane which satisfies condition (2). This gives us reason enough to be curious and investigate whether the circular jump actually demonstrates horizon effects or not. Let us probe that experimentally.

3. Designing the Experiment

Admittedly, to observe a circular hydraulic jump, one does not require an extraordinary amount of engineering - opening a tap in the kitchen sink suffices. However, to ensure laminar flow and perfect circular rings and eliminating other kinds of perturbations, one needs to be careful in their experimental approach. In this section, I describe how the experiment was set-up.

Figure 3: Actual set-up assembled in the Hydrodynamics lab for the purposes of the project

---

[5]Interestingly, any spherically symmetric geometry can always be put in a coordinate system where the space is flat and all spacetime curvature is forced into the g_{tt} and g_{ti} components of the metric.

3.1 *Experimental Set-Up*

The two primary things that were required were a nozzle with fluid flow and an impact plate. The rest of the set-up was designed around these two components. First, we decided to use an overhead tank attached to a faucet kept above a glass plate. Then, the glass plate was kept inside a tray in which we drilled two holes for draining the fluid. Next, we attached levelling screws to the bottom of the tray to ensure that the tilt in the glass plate was not deforming the shape of the circular jump. Under the tray, we decided to keep a lighting panel in order to illuminate the pictures of the circular jump in a diffused fashion and improve the visibility of the jump radius. Next, we immersed a pipe connected to an electric pump[6] which pumped the liquid back to the overhead tank. We put a transparent graph sheet on top of the glass for calibrating scale in the measurements. To ensure that the vibrations of the motor did not affect the circular jump, the motor was kept on a different table and the pipe pumping the liquid was held up by an independent frame not touching the glass-plate table. By varying the current provided to the motor, we could change the flow rate of the pump. At different flow rates, the liquid achieved a dynamic equilibrium at different levels on the overhead tank. By achieving a constant fluid height on the overhead tank, we could deduce a constant flow rate for the open nozzle. As the liquid impacted the glass plate at a given value of flow rate Q, we clicked pictures of the circular jump. A cartoon diagram of the set-up has been provided in Fig. 4 and actual images of the set-up are displayed in Fig. 3.

3.2 *Resolved Experimental Challenges*

During the course of the experiment, I faced a couple of challenges - some quite unrelated to fluid mechanics and general relativity.

1. **Low out-flow rate leading to flooding of the tray.** This was overcome by drilling an additional hole for draining the liquid and creating an opening in the draining pipes in order to let out air.

2. **Oscillations of the circular jump.** A number of measures were taken to eliminate this. Two subtle changes that had to be incorporated were shifting from a peristatic pump to an centrifugal pump and suspending the pipe bringing fluid to the overhead tank on an external frame. Additionally, the tip of the pipe was encased in a solid PVC tube help up by a retort stand to further minimize any of the vibrations which were leaking into the tank.

3. **Noisy edges of the circular jump.** The immediate change that was adopted was to move to a more viscous liquid. First we tested the set-up for its flow using water. Then, we used glucose solution to test for higher density higher viscosity liquids. Finally, we adopted silicone oil once we were reasonably confident about the functioning of the apparatus.

---

[6]During the initial stages of the experiment, we used a peristatic pump but then later we shifted to a horizontal centrifugal pump due to its reduced vibrations
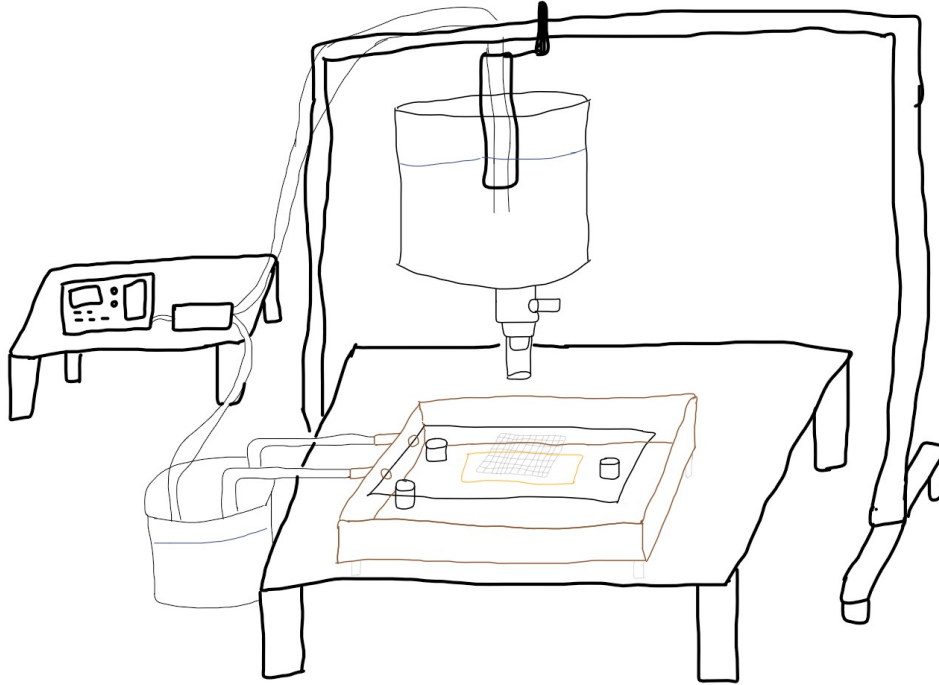
Figure 4: A simplified diagram to illustrate the main components of the experimental set-up.

4. **Lack of clear edges while analysing images.** We tried a variety of different lighting angles and forms until we realized that a bottom up illumination diffused by the material of the tray provided optimal results.

3.3 *Unresolved Experimental Challenges*

part of what we wish to demonstrate is that the surface velocity v_s is greater than the ripplon phase velocity v_p inside the circular jump. One way to do so would be to measure v_s and v_p inside and outside the horizon. However, there are several challenges associated with it.

1. Inside the circular jump, the surface flow is very rapid and, therefore, any bead kept inside is immediate pushed out. My intuition at first was to aerate the silicone oil in the overhead tank to some extent and then take a video to analyze the motion of air bubbles. However, discerning air bubbles in trackpy was a very difficult task.

2. The height of the liquid inside the jump can be upto an order of magnitude lower than the surrounding film. Therefore, solid objects like thermocol balls perturb the surface flow too much by changing the geometry.

3. We also wanted to know the phase velocity near the horizon. In principle this can be done by sending a wave. Though instructive for pedagogical purposes, for precision experimenting

this leads to the popular backreaction problem i.e. a test signal changes the background field thereby changing the measurement result in intractable ways.

Fortunately for us, we can demonstrate that the surface velocity moves from sub-luminal (i.e. slower than phase velocity) to super-luminal (i.e. faster than phase velocity) without explicitly measuring the two quantities separately.

4.   **Experiment's Results**

Note that all subsequent measurements have been taken using silicone oil of 20 cst viscosity.

4.1   *Data Processing*

First, we collected data for the dependence of jump radius R with respect to flow rate Q. The data collected for this part has been demonstrated in Fig. 5. These results match - in the order of magnitude - the results achieved by Jannes et al. (though under slightly different experiment parameters).
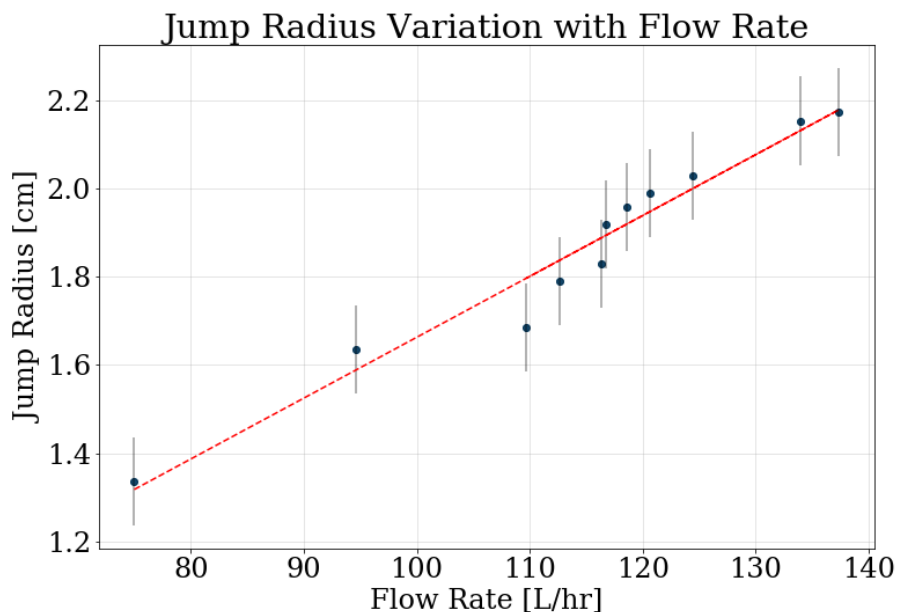
Figure 5: Varying radius of circular hydraulic jump by changing the flow rate of the liquid.

Next, once the ability to achieve constant flow and measuring of radial distance was verified, I used a sharp point like perturbation to artificially create mach cones in the fluid flow (see. Fig. **??**). Though we do not have a faster than ripplons object travelling in the fluid, if the fluid itself moves faster than ripplons next to a stationary object, by principle of relativity we should get the same

results. I took one continuous video of my sliding the obstruction closer to the center of the jump and then analyzed the frames of that video on ImageJ to measure the angles. These results have been plotted in Fig. 7.
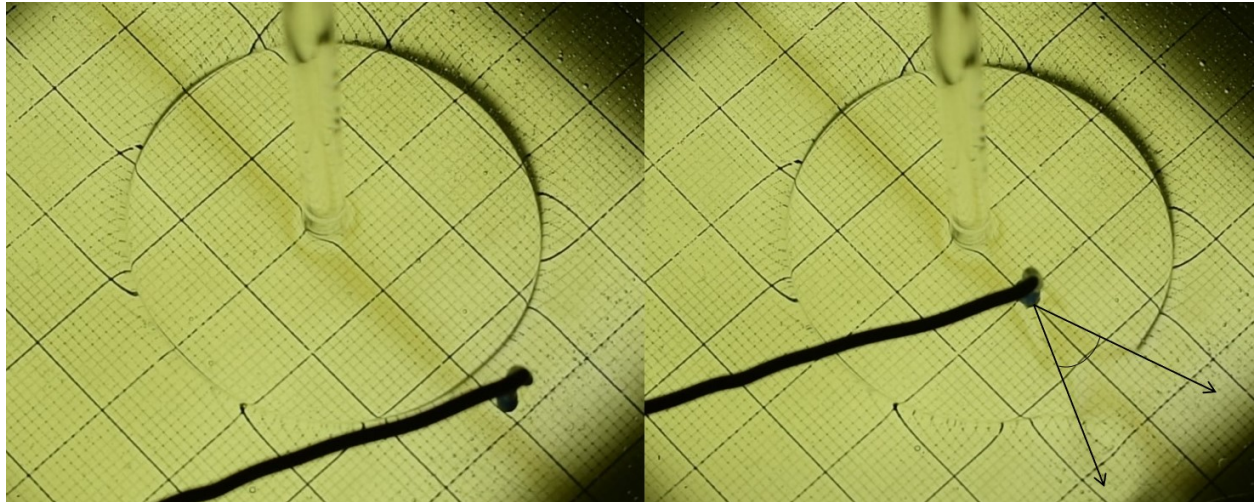
Figure 6: Appearance of Mach Cones as the poin like perturbation is dragged inside the jump radius.
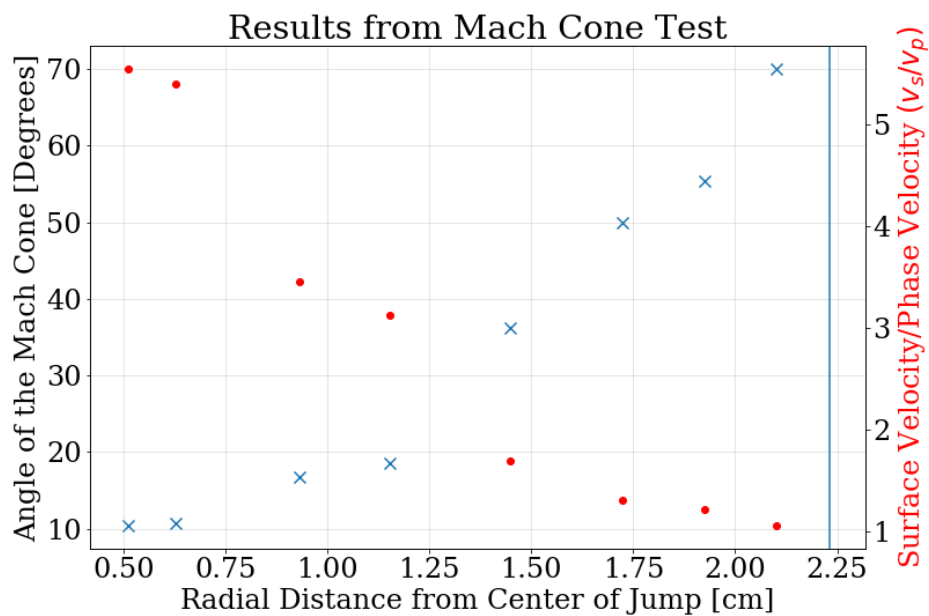
Figure 7: Measuring the mach cone angles created by artificial obstruction inside the circular jump. Vertical blue line represents the jump radius.

In Fig. 7, the Y-axis on the right has been calculated simply using the relation between mach angle (i.e. the half angle of the mach cone) and the ratio of velocities i.e. $v_p/v_s = 1/\sin\theta$ which can be easily derived using simple trigonometry on mach cones.

4.2 *Inferences*

First, let us recall the PG metric which described the circular jump.

$$g_{\mu\nu}^{ripplon} \propto \begin{pmatrix} -(v_p^2 - v_s^2) & -(v_s)_i \\ -(v_s)_i & \delta_{ij} \end{pmatrix} \tag{90}$$

The condition for getting a horizon is to have the g_{tt} component of the metric be zero. This implies that for the case of horizon, $v_s = v_p$. In terms of the mach angle, we get $\theta = \sin^{-1}(1) \implies \theta = 90º$. We can clearly see that Fig. 7 clearly demonstrates that the mach cones have precisely this asymptotic behavior. So, not only have we qualitatively demonstrated the existence of super-luminal (greater than ripplon phase velocity) fluid flow inside the circular hydraulic jump but also demonstrated the existence of a horizon that coexists with the physical discontinuity at the jump radius.

Moving ahead, we can look at the fact that a higher flow rate leads to a bigger jump radius. This means higher flow rate effectively pushes the circular jump's horizon further away. Now, one might be tempted to draw parallels with the fact that the more massive a Schwarzschild black/white hole is, the bigger is its Schwarzschild radius $r_s = 2GM/c^2$. However, one must acknowledge the fact that the mass and energy coupling with the curvature of spacetime is a dynamical behavior of general relativity (i.e. it relates to Einstein's field equations).

Spacetime's corresponding element in fluid mechanics is the background flow which is constrained by Euler equation and Continuity equation. Spacetime in general relativity, however, needs to follow no such constraints. Therefore, *a priori* we only have reason enough to draw parallels between kinematic features of GR with our analog models. Effectively, this means we can emulate geometries and study the geodesic motion of particles but there is uncertainty when it comes to studying the correspondence of the geometries with their source.

5. Scope for Further Work

In terms of the experimental aspects of this project, there are a couple of short term results that I wish to collect from the existing set-up without any modification.

1. Change in jump radius with respect to height of the overhead tank.

2. Change in jet radius with respect to flow rate.

3. Mach cone angles for varying jump radius.

4. Adding colored silicone beads to get order of magnitude estimate of flow velocities.

These extra data points do not contribute in any significant manner to new conceptual aspects of the project but would help increase the level of confidence about the existing claims in this report.

Further, as mentioned earlier, any spherically symmetric spacetime can be made to fit into the Painleve-Gullstrand coordinate form. Therefore, it is worth investigating if Kerr blackhole metrics too have interesting analog properties in fluid mechanics. Additionally, nozzle geometries are also easily reproducible analogs to black hole spacetimes as hydraulic jumps are to white-hole spacetimes. In such cases, considering gravitational lensing too is a purely kinematic phenomena, we expect that the incoming wavefront of ripplons might demonstrate predictable lensing behavior which may have correspondence with null geodesic deviations in GR spacetimes.

Finally, one of the primary open questions in the field of analog gravity is that of Hawking Radiation. Since Hawking Radiation is an entirely kinematic feature of general relativity (in the sense that it can be derived without referring to Field equations at all), there is value in exploring what parts could be a good exercise in teaching myself the relevant details of quantum field theory in curved spacetime and Hawking's derivation of Hawking radiation.

6. Conclusion

Over the course of this project, I explored how the equations of fluid mechanics - in certain sense - can demonstrate corresponding maps to features of general relativity. As per the analytic treatment, we expected hydraulic circular jumps to show horizon effects similar to Schwarzschild geometry. To confirm this hypothesis, we designed and conducted an experiment using silicone oil and by studying the angles of mach cones produced, we observed desired signatures of horizon effects.

Works Cited

[1]   P. Bhagat R. Linden. "The Circular Capillary Jump." In: (Mar. 2020).

[2]   Faccio D. et al. *Analogue Gravity Phenomenology*. Springer, 2013.

[3]   Jannes G. et al. "Experimental demonstration of the supersonic-subsonic bifurcation in the circular jump: A hydrodynamic white hole." In: *Physical Review* (2011).

[4]   Jannes G. et al. "Horizon effects for surface waves in wave channels and circular jumps." In: *Journal of Physics: Conference Series* (2011).

[5]   R. Fitzpatrick. *Theoretical Fluid Mechanics*.

[6]   G. E. Volovik. "Horizons and Ergoregions in Superfluids." In: (2006).

[7]   G. E. Volovik. "Hydraulic Jumps as a White Hole." In: *JEPT Letters* (2005).